© 2020. Published by The Company of Biologists Ltd | Journal of Cell Science (2020) 133, jcs238709. doi:10.1242/jcs.238709

RESEARCH ARTICLE

Translesion synthesis polymerases contribute to meiotic chromosome segregation and cohesin dynamics in *Schizosaccharomyces pombe*

Tara L. Mastro*, Vishnu P. Tripathi and Susan L. Forsburg‡

ABSTRACT

Translesion synthesis polymerases (TLSPs) are non-essential error-prone enzymes that ensure cell survival by facilitating DNA replication in the presence of DNA damage. In addition to their role in bypassing lesions, TLSPs have been implicated in meiotic double-strand break repair in several systems. Here, we examine the joint contribution of four TLSPs to meiotic progression in the fission yeast *Schizosaccharomyces pombe*. We observed a dramatic loss of spore viability in fission yeast lacking all four TLSPs, which is accompanied by disruptions in chromosome segregation during meiosis I and II. Rec8 cohesin dynamics are altered in the absence of the TLSPs. These data suggest that the TLSPs contribute to multiple aspects of meiotic chromosome dynamics.

KEY WORDS: DNA repair, Meiosis, Translesion synthesis, *S. pombe*, Rec8, DDK

INTRODUCTION

Faithful transmission of genetic information across generations relies upon high fidelity polymerases during DNA synthesis. These are largely error free due to 3′–5′ proof-reading activities (Prakash et al., 2005; Rattray and Strathern, 2005). However, these replicative polymerases are unable to synthesize beyond helix distorting lesions such as abasic sites, base dimers, and bulky adducts (Prakash et al., 2005; Rattray and Strathern, 2005). Rather, the replicative polymerase will stall potentially leading to deleterious double-strand breaks or fork collapse (Alexander and Orr-Weaver, 2016; Zeman and Cimprich, 2014).

Translesion synthesis polymerases (TLSPs) are capable of synthesis beyond distorting lesions at the cost of being error prone. Many have error rates exceeding one in one thousand (Goodman, 2002). However, this allows DNA synthesis and cell cycle progression to continue (Waters et al., 2009). TLSPs also contribute to genomic stability by gap filling (Heller and Marians, 2006). There are now well over a dozen described TLSPs in human cells, several of which are conserved in the budding and fission yeasts (Prakash et al., 2005; Rattray and Strathern, 2005). In budding yeast two TLSPs, Polζ and Rev1, initiate microhomology-mediated break-induced replication (MMBIR), especially in cases where break-induced replication pathways are inactivated (Sakofsky et al., 2015). MMBIR allows for cell survival by preventing replication failure, but has the consequence of creating complex genomic rearrangements that are implicated in many human diseases (Carvalho et al., 2010; Hastings et al., 2009; Liu et al., 2012; Ottaviani et al., 2014; Sakofsky et al., 2015). Evidence suggests that TLSP function is regulated in part by the conserved DDK kinase that is active in S phase (Brandão et al., 2014; Day et al., 2010). Increasing the expression of TLSPs causes hypermutation (Bavoux et al., 2005; Bergoglio et al., 2002; Kim et al., 1997; Ogi and Lehmann, 2006). Thus, TLSPs are a double-edged sword, requiring careful regulation to preserve genome stability.

Fission yeast has four known TLSPs: Rev1, Pol ζ, Eso1, and Pol κ (also known as Mug40 and Kpa1) (Deshpande et al., 2009; Kai and Wang, 2003; Tanaka et al., 2000). These are not essential for viability but contribute to DNA repair and genome integrity (Callegari and Kelly, 2016; Callegari et al., 2010; Coulon et al., 2010; Tanaka et al., 2000). Eso1 is unique in *Schizosaccharomyces pombe* in that it is a gene fusion of two proteins that are encoded separately in other organisms, the essential cohesin acetyltransferase Eco1, and DNA Pol η (also known as Rad30 in budding yeast and POLH in mammals); this compound protein might be split post-translationally (Chen et al., 2014; Tanaka et al., 2000).

Meiosis is a differentiation pathway that reduces diploid cells to haploid gametes. A key feature of meiosis in most eukaryotes is the process of genetic exchange through physical recombination (Hochwagen, 2008; Ohkura, 2015). Previously, a connection between TLSPs and meiosis in *S. pombe* was shown through the regulatory subunit of the DDK kinase, Dfp1 (also known as Him1; Le et al., 2013). Dfp1 is required for the error prone pathway of post-replication repair (PRR) where the TLSPs also function (Le et al., 2013). A truncation allele, *dfp1-r35*, is defective in induced mutagenesis, indicating that it has a role in TLSP activity. This mutant also has striking defects in meiosis, including disruptions of replication, induction of programmed double-strand breaks and chromosome segregation (Le et al., 2013).

A role for TLSPs in meiosis can be inferred, because their gene expression is increased in synchronous *S. pombe* meiotic cells (Mata et al., 2007). This increase is even more profound than that seen in many environmental stress situations such as H_2O_2 treatment (Chen et al., 2003; Kawamoto et al., 2005; Mata et al., 2007). Transcriptional upregulation in meiotic cells is not limited to fission yeast. In humans and mice, *pol η* has enriched expression in the testis, specifically in the spermatotids in the mouse (McDonald et al. 1999). This transcriptional upregulation may be indicative of a meiotic role for these polymerases.

One attractive model for a meiotic function of TLSPs may be meiotic double-strand break repair. Two studies have demonstrated *in vitro* that Pol η can perform D-loop extension during homologous recombination (HR) in double-strand break repair (DSB) using

Department of Biological Sciences, University of Southern California, Los Angeles, CA 90089-2910, USA.
*Present address: Division of Biology and Biological Engineering, California Institute of Technology, 1200 East California Blvd, Pasadena, CA 91125, USA.

‡Author for correspondence (forsburg@usc.edu)

V.P.T., 0000-0002-6137-8547; S.L.F., 0000-0002-4895-8598

Handling Editor: David Glover
Received 4 September 2019; Accepted 26 March 2020

Journal of Cell Science (2020) 133, jcs238709. doi:10.1242/jcs.238709

either purified human or budding yeast Pol η (Li et al., 2009; McIlwraith et al., 2005) indicating that the ability of Pol η to perform D-loop extension is conserved. In budding yeast, TLSPs contribute to mutagenesis during HR in meiosis, potentially aiding in genetic diversification (Arbel-Eden et al., 2013).

In this study we investigate the role of TLSPs in *S. pombe* meiotic progression. We describe a phenotype of chromosome mis-segregation due to the simultaneous loss of all four TLSPs in *S. pombe*. Furthermore, we show that these TLSPs do not substantially affect meiotic DSB repair and recombination. Rather, our data suggest a combined role in cohesion dynamics.

RESULTS

Spore viability is reduced in TLSP mutants

In order to determine the magnitude of contribution to meiotic progression, if any, of the TLSPs in *S. pombe,* we analyzed spore viability using random spore analysis. The largest reduction in spore viability was in the quadruple TLSP mutant lacking all four proteins (Fig. 1A). Each single TLSP mutant showed a modest, but statistically significant reduction in spore viability. *eso1*Δ*η* (deletion of the *pol η* homology region only) and *rev1*Δ had similar reductions in viability compared to the viability of wild type, to 64% and 61% respectively. *kpa1*Δ showed a very modest reduction to 81% of wild-type viability, whereas *rev3*Δ (encodes a subunit of Pol ζ) had a 47% relative viability. The quadruple mutant, which we termed *quad*Δ, showed a reduction to 16% relative viability. This is comparable to the 19% relative viability observed in *rec12*Δ, which fails to make meiosis-specific DSBs and thus lacks all recombination (Fig. 1A) (Sharif et al., 2002). We observed little to no reduction in mitotic viability, as assessed by plating efficiency, in any single mutant or in the quadruple mutant, which indicates that the failure to observe spore colonies is not due to mitotic defects during spore outgrowth, but likely represents a failure in meiosis (Fig. 1B).

Each mutant had a characteristic sensitivity to DNA damaging agents during vegetative growth (Fig. 1C). We observed, as was previously reported, that *eso1*Δ*η* shows enhanced sensitivity to ultraviolet radiation (Tanaka et al., 2000). *kpa1*Δ showed enhanced sensitivity to the alkylation damage from methyl methanesulfonate (MMS), which is consistent with a predicted role in nucleotide excision repair (Ogi and Lehmann, 2006). In contrast, *rev3*Δ had a significant sensitivity to the topoisomerase inhibitor, camptothecin (CPT), which causes S phase specific breaks by inhibition of topoisomerase (Ryan et al., 1994). Unexpectedly, *rev1*Δ had sensitivity to the spindle poison, thiabendazole (TBZ), which is typically seen for mutants affecting mitotic segregation. Interestingly, the *quad*Δ showed a less severe phenotype when challenged with CPT and TBZ compared to single mutants (*rev3*Δ and *rev1*Δ, respectively). It appears that in some situations the lack of all four of the polymerases is less deleterious than the absence of one.

The quadruple TLSP mutant has normal meiotic recombination, DSB repair, and progression

There is increased expression of fission yeast TLSPs in meiosis but with differing timings (Mata et al., 2007). Kpa1 and Eso1 are expressed early in the meiotic program, during meiotic DNA synthesis, while Rev1 and Rev3 reach a maximum around meiosis I (MI) and meiosis II (MII). We examined whether the spore viability defect in the *quad*Δ reflects defects in recombination, which occur early in the meiotic program. In *rec12*Δ cells that completely lack meiotic DSBs, there is a loss of spore viability to 19% that of wild type, which is similar to that of the quadruple deletion mutant (Fig. 1A) (Pankratz and Forsburg, 2005; Sharif et al., 2002). In contrast, if meiotic DSBs are made, but there is a catastrophic failure of DSB repair, spore viability drops to near zero (Boddy et al., 2001; Catlett and Forsburg, 2003; Cromie et al., 2006; Lorenz et al., 2012; Osman et al., 2003). We examined the formation of DSBs using pulse-field gels of whole chromosomes from a diploid where synchronous meiosis was induced using the *pat1-114* temperature sensitive allele (Mastro and Forsburg, 2014; Pankratz and Forsburg, 2005). In wild-type cells, meiotic DSBs were visualized as a smear below the intact chromosomes. These occurred between 3 and 4 h and were resolved by 5 h. This trend was similar in wild type and *quad*Δ (Fig. 2A). Thus, there appears to be no gross disruption in meiotic DSB occurrence or repair dynamics in the absence of all four TLSPs. Consistent with this, the overall timing of pre-meiotic S phase and meiotic divisions were similar in both wild type and *quad*Δ, as measured by timing of nuclear divisions and meiotic S phase (Fig. 2B,C).

Next, we examined the resolution of the breaks by examining inter-homolog recombination between two markers on chromosome II that are approximately 76 kb apart. In wild-type cells this resolved as a genetic distance of 8.34 cM. All the single and quadruple mutant TLSPs maintained similar levels of recombination as the wild type with no significant differences with the exception of *kpa1*Δ, which had a slight reduction in homolog recombination in this interval (Fig. 2D,E). Thus, the defects causing failure of meiosis are not due to gross defects in the program of meiotic recombination.

The quadruple TLSP mutant has disrupted chromosome segregation in meiosis

We examined the dynamics of meiotic progression using live-cell imaging of a normal diploid (i.e. not induced by *pat1*). We used a strain where one copy of chromosome I carries a *lacO* array adjacent to the centromere, and that expresses LacI–GFP and histone H3 tagged with mRFP (H3–mRFP) (Tomita and Cooper, 2007). We observed that the *quad*Δ generated additional H3–mRFP bodies during MI and MII divisions (10.47% and 13.25% of divisions, respectively) (Fig. 3A–D; Movie 2). This could be due to fragmentation or mis-segregation. MI and MII fragmentation was significantly less frequently observed in wild type compared to the *quad*Δ [3.76% and 3.88%, respectively (P=0.046 and P=0.013; Fisher's exact test)] (Fig. 3A–D; Movie 1). There was also a significant increase in any type of meiotic abnormalities during MI (i.e. uneven segregation or fragmentation) in the *quad*Δ compared to in wild type (P=0.0036 and P=0.0065, respectively) (Fig. 3A–D; Movies 1,2). We also observed an increase in the frequency of unequal nuclear divisions during MI and MII in *quad*Δ (MI=10.47% and MII=3.61%) compared to in wild type (MI=0.75% and MII=0.00%) (Fig. 3A–D). Taken together, these observations suggest defects in overall chromosome segregation, which could represent chromosome fragmentation, nondisjunction, or premature sister chromatid separation.

We monitored LacI–GFP foci associated with a *lacO* array integrated proximal to the centromere in one copy of chromosome I to distinguish reductional (MI) versus equational (MII) division. During MI division (reductional) in wild type, the sister chromatids remain associated while the labeled and unlabeled homologs separate, so the LacI–GFP focus remains in a single nucleus. In the MII division (equational), the sister chromatids segregate, leading to separation of two LacI–GFP foci into adjacent spores. The reductional and equational divisions are dependent on meiotic cohesin Rec8, and its step-wise cleavage (Yokobayashi et al., 2003). In a *rec8*Δ mutant, the absence of proper cohesion at the centromere leads to an equational MI division and premature sister chromatid

Journal of Cell Science (2020) 133, jcs238709. doi:10.1242/jcs.238709

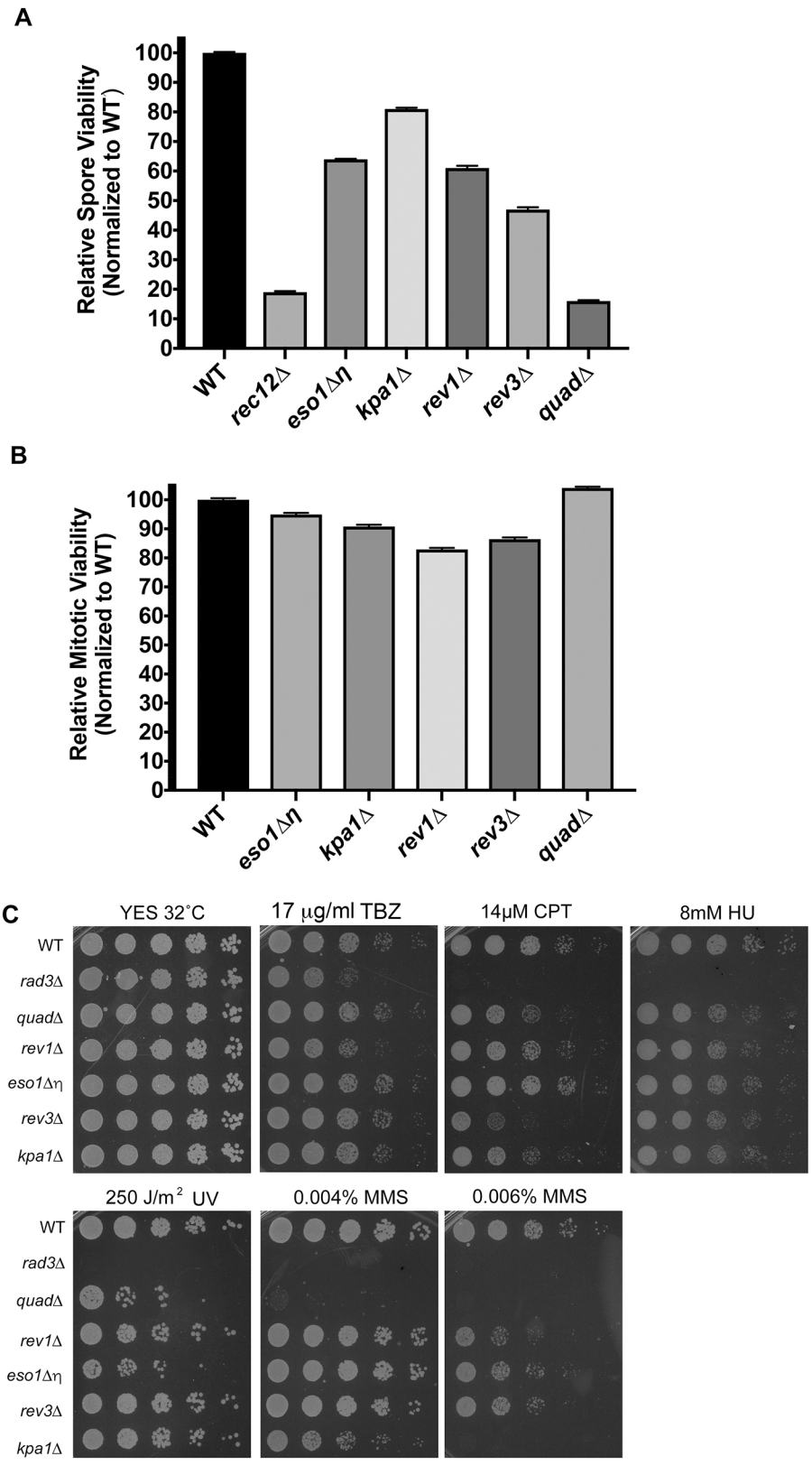

Fig. 1. Spore and mitotic viability. (A) Spore viability relative to wild type (WT) was analyzed via random spore analysis by plating the following number of spores for each sample group: WT (1251×5207)=27,800, *rec12*Δ (4561×5268)=7800, *eso1*Δ*η* (5262×5269)=6800, *kap1*Δ (7616×7685)=12,000, *rev1*Δ (5401×5466)=4000, *rev3*Δ (5259×5263)=4000 and *quad*Δ (6664×6716)=8500. Data was pooled between technical and biological replicates and analyzed as categorical data. Data shown are mean±s.e.m. calculated for categorical data. (B) Mitotic plating efficiency relative to wild type was determined by plating the following number of cells for each group: WT (1251, 5207)=9000, *eso1*Δ*η* (5262)=9000, *kap1*Δ (5258, 5270)=6000, *rev1*Δ (5401, 5466)=9000, *rev3*Δ (5259, 5263)=7500 and *quad*Δ (6664, 6716)=9500. Data was pooled between technical and biological replicates and analyzed as categorical data. Data shown are mean±s.e.m. calculated for categorical data. (C) Long-term drug sensitivity assays (YES, untreated control; HU, hydroxyurea). *rad3*Δ (3070) is shown as a positive control and WT is the negative control for the drug plates. Other strains shown are *eso1*Δ*η* (5262), *kap1*Δ (5258), *rev1*Δ (5466), *rev3*Δ (5259) and *quad*Δ (6716). Cells plated in 5× serial dilutions on minimal medium containing the concentrations of the indicated drugs are shown. The images are representative of three biological replicates each with two technical replicates. Strain numbers for strains used and for parental strains in crosses are given in brackets, see Table S1 for details.

separation (Yokobayashi et al., 2003). Conversely, if there is a failure of Rec8 cleavage so that the protein persists, the sisters will not separate during MII, and this nondisjunction resembles a reductional division (Kitajima et al., 2003). The *quad*Δ strain showed a statistically significant increase in nondisjunction or non-separation in MII compared to wild type (P=0.0026) but not in MI, indicating a failure to segregate sister chromatids properly during the equational division (Fig. 3B,E).

Next, we asked whether the additional histone signals observed in the LacI–GFP/H3–mRFP co-expression experiments are whole

Journal of Cell Science (2020) 133, jcs238709. doi:10.1242/jcs.238709

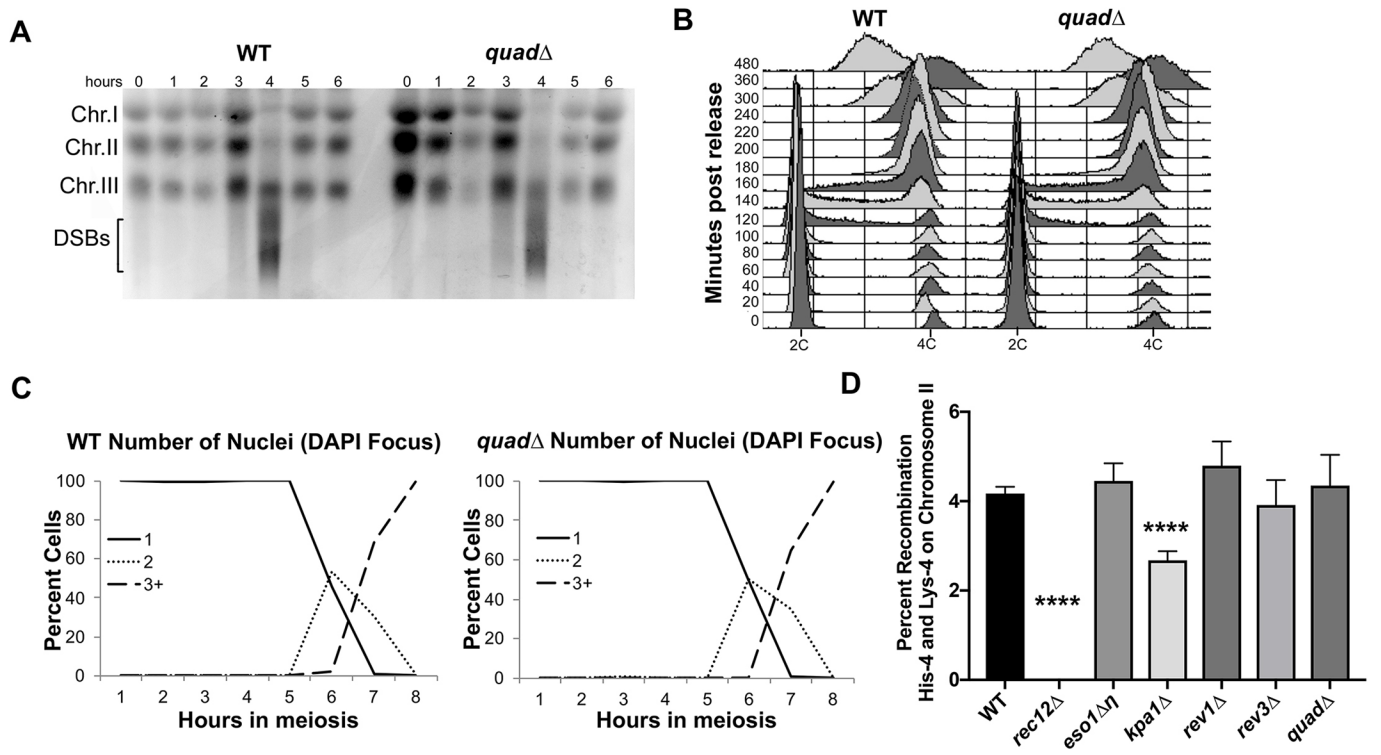

E

Map distance between His-4 and Lys-4 on Chromosome II							
	WT	*rec12Δ*	*eso1Δη*	*kpa1Δ*	*rev1Δ*	*rev3Δ*	*quadΔ*
cM	8.34	0	8.91	5.35	9.59	7.83	8.70

Fig. 2. Recombination and synchronous meiosis. (A) Representative image of three biological replicate pulse-field gel electrophoresis experiments showing chromosomes I, II, and III with lower molecular weight programmed meiotic double-strand breaks for wild type (WT; 2057×3500) and *quad*Δ (6671×7117). (B) Flow cytometry data showing replication progression during meiotic time course. Data shown are representative of at least three biological replicates. (C) DAPI staining of meiotic progression of 1, 2 and 3+ DAPI-stained nuclear masses, representative of three biological replicates for WT (2057×3500) and *quad*Δ (6671×7117). (D) Graph of meiotic recombination frequency between *his4-239* and *lys4-95* on chromosome II. The sample size for each group is as follows: WT (1251×5207)=17,714, *rec12*Δ (4561×5268)=969, *eso1*Δ*η* (5262×5269)=2762, *kap1*Δ (7616×7685)=6169, *rev1*Δ (5401×5466)=1201, *rev3*Δ (5259×5263)=1544 and *quad*Δ (6664×6716)=874. Data was pooled between technical and biological replicates and analyzed as categorical data. Data shown are mean±s.e.m. calculated for categorical data. Fisher's exact test was used to determine significance compared to WT (*rec12*Δ $P<0.0001$, *eso1*Δ*η* $P=0.4762$, *kpa1*Δ $P<0.0001$, *rev1*Δ $P=0.7092$, *rev3*Δ $P=0.2354$, *quad*Δ $P=07,948$; ****$P<0.0001$). (E) Genetic distance in cM between His-4 and Lys-4 on chromosome II for WT and mutants, as calculated using the following formula: (2(His$^+$Lys$^+$)/total colonies)×100. Strain numbers for parental strains in crosses are given in brackets, see Table S1 for details.

chromosomes or fragments. We examined segregation in a strain with H3-mRFP and the telomere protein Taz1 tagged with GFP (Taz1–GFP). We reasoned that whole chromosomes would always contain a telomere, but a chromosome fragment might not. It was previously shown that mutants that suffer from failures in DSB repair have mis-segregating histone signals that lack Taz1–GFP signals, while mutants with failures in whole chromosome separation, such as *rec12*Δ, have a Taz1–GFP signal on the mis-segregating histone body (Mastro and Forsburg, 2014). We observed a difference in Taz1–GFP signal between MI and MII mis-segregations in the *quad*Δ (Table 1). Only 55% of mis-segregated histone bodies had a Taz1–GFP signal associated, suggesting that a fraction of these are some sort of chromosome fragmentation, whereas all MII mis-segregating histone bodies had at least one Taz1–GFP signal, suggesting that these segregations involve a whole chromosome.

Rec8–GFP dynamics and recruitment are altered in *quad*Δ

We reasoned that uneven chromosome segregation and failed equational divisions in the *quad*Δ mutant could reflect disruptions or misregulation of the meiosis-specific cohesin Rec8. We have previously shown that the DDK regulatory subunit Dfp1 contributes to the error prone TLS pathway in mitotic cells, and also that disruption of *dfp1* results in misregulation of Rec8 (Dolan et al., 2010; Le et al., 2013). DDK also interacts with the Swi1–Swi3 proteins in the fork protection complex, mutants of which also have a meiotic defect (Escorcia and Forsburg, 2017). We examined the dynamics of Rec8–GFP using live-cell imaging of asynchronous diploid meiotic cultures.

Rec8 has very characteristic visual patterns as cells go through meiosis (Escorcia and Forsburg, 2017; Mastro and Forsburg, 2014; Watanabe et al., 2001). As seen previously, we observed that wild-type cells show a pan-nuclear signal which is reduced to two single puncta shortly following the MI division, indicating Rec8–GFP had been released from the chromosome arms but maintained at the centromeres (Fig. 4A; Movie 3) (Escorcia and Forsburg, 2017; Le et al., 2013; Watanabe and Nurse, 1999). These puncta disappeared just prior to MII, indicating that Rec8–GFP had been fully removed from the chromosomes. These dynamics are dramatically altered in the *quad*Δ mutant. There was a modest but significant delay in the disappearance of the pan-nuclear signal in

Journal of Cell Science (2020) 133, jcs238709. doi:10.1242/jcs.238709

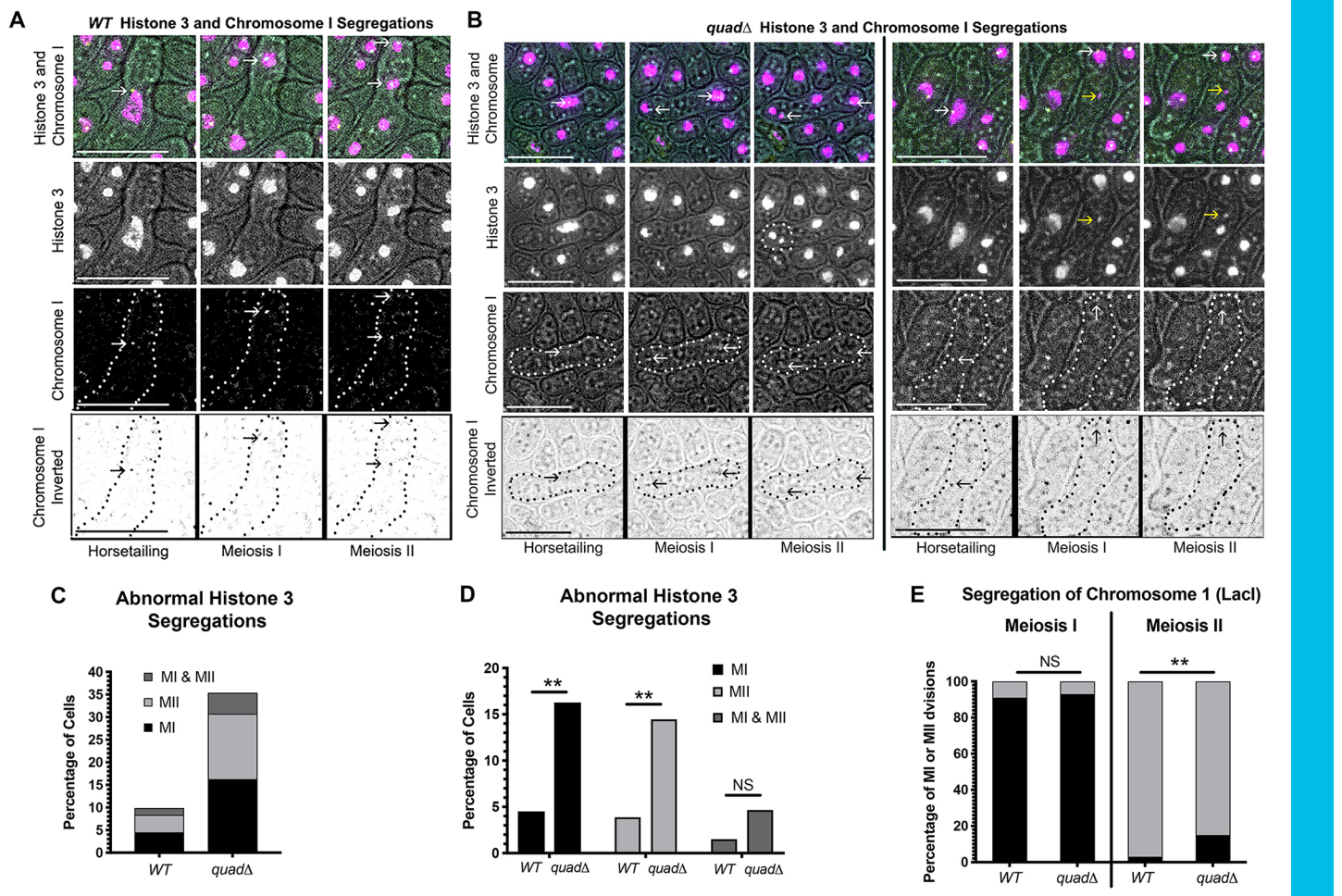

Fig. 3. Meiotic chromosome segregation. Quantification of meiotic abnormalities for wild type (WT; 5608×5787) and *quad*Δ (7168×7117). (A,B) Meiotic abnormalities include histone fragments during segregation and uneven nuclear segregations. Scale bars: 10 µm. (A) Representative images showing H3–mRFP and LacI–GFP on chromosome I for WT (MI, *n*=133; MII, *n*=129). The top row shows H3 and LacI on chromosome I. Second row shows H3. The third and fourth rows show LacI–GFP signals binding to the *lacO* on chromosome I. The dotted outlines represent the cell boundary and arrows indicate the LacI signals. (B) Representative images showing *quad*Δ (MI, *n*=86; MII, *n*=83), as in A. The black and white arrows indicate LacI signals and the yellow arrows indicate fragmented H3 signals. In the second row, an uneven segregation event is indicated by a dotted circle. In the third and fourth row the cell boundary is indicated with a dotted line. (C,D) Quantification of meiotic errors observed in live-cell imaging. Significance was calculated using a Fisher's Exact Test (MI, *P*=0.0036; MII, *P*=0.0065; MI and MII, *P*=0.1643; ***P*<0.01; NS, not significant). (E) Quantification of LacI–GFP segregation in MI and MII. The percentage of MI or MII divisions that were reductional is shown in black, and the percentage of divisons that were equational is shown in gray. Significance was calculated using a Fisher's Exact test (MI, *P*=0.793; MII, *P*=0.0026; ***P*<0.01; NS, not significant). Data in C–E are from experiments that tracked individual cells (WT MI, n=133; WT MII, n=118; *quad*Δ MI, n=87; *quad*Δ MII, n=80). Strain numbers for parental strains in crosses are given in brackets, see Table S1 for details.

the *quad*Δ mutant compared to disappearance in the wild type (17 and 10 min, respectively). Conversely, we observed that *quad*Δ had a significantly shorter duration of the Rec8–GFP foci compared to that in wild type (32 min and 55 min, respectively) (Fig. 4B; Movie 4). This suggests there may be a delay in the removal of Rec8 from chromosome arms during MI, but that it may be prematurely removed from the centromere during MII. The premature loss of Rec8–GFP in MII was also seen in the absence of replication fork mutants *swi1* and *swi3* (Escorcia and Forsburg, 2017).

Table 1. Taz1–GFP signal for *quad*Δ (7691×7692) H3–mRFP mis-segregating bodies

Type of H3–mRFP Body	MI	% MI	MII	%MII
Taz1–GFP-plus	11	55	20	100
Taz1–GFP-minus	9	45	0	0
Total	20		20	

Rec8 dynamics are regulated through phosphorylation. Phosphorylation by the kinases DDK and CK1 is required for Rec8 cleavage at the centromere (Ishiguro et al., 2010; Le et al., 2013). In contrast, dephosphorylation by Sgo1–PP2A prevents Rec8 cleavage (Ishiguro et al., 2010). We examined Rec8–GFP phosphorylation and overall protein levels through meiosis in a *pat1-114*-driven synchronous meiosis in diploids (Fig. 4D) (Bähler et al., 1991; Escorcia and Forsburg, 2017; Le et al., 2013; Mastro and Forsburg, 2014). Using the completion of MI as time 0 h, Rec8–GFP was visible at −4 h through to 2 h, with the slower migrating phosphorylated species present in wild type at −2 h through to −1 h (Le et al., 2013; Parisi et al., 1999; Rumpf et al., 2010). The phosphorylation at one hour prior to MI in the *quad*Δ mutant was modestly reduced compared to that in wild type (*P*=0.0317) (Fig. 4C,D; Fig. S1). There was no significant change in Rec8–GFP levels between wild type and *quad*Δ when Rec8–GFP was compared to total protein, although there was a trend of the *quad*Δ

Journal of Cell Science (2020) 133, jcs238709. doi:10.1242/jcs.238709

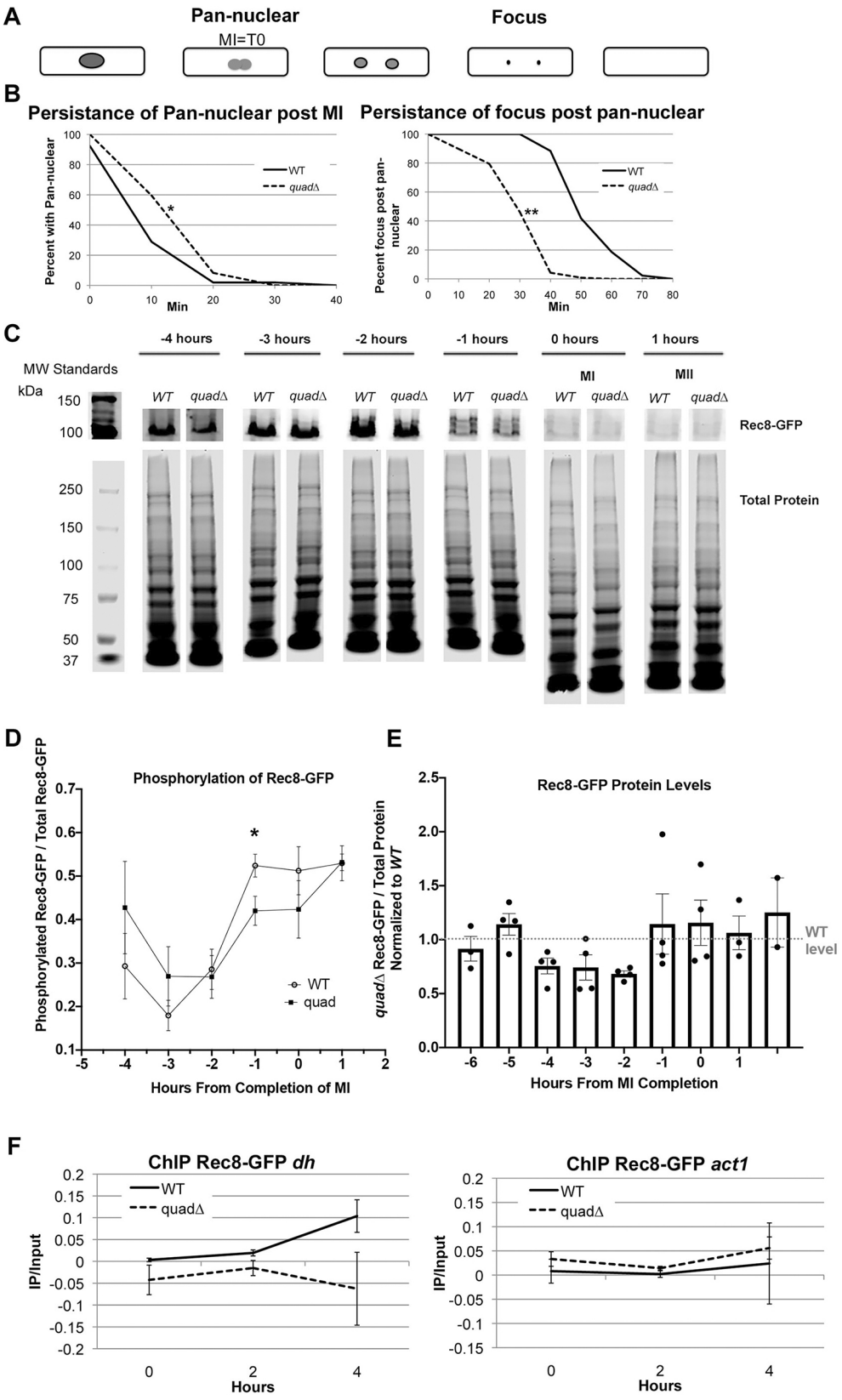

Fig. 4. Rec8 dynamics. (A) Live-cell imaging of Rec8–GFP; schematic of pan-nuclear versus focus formation during meiosis for wild type (WT; 6137×6138) and *quad*Δ (7428×7402). (B) Quantification of the Rec8–GFP live-cell imaging. For WT, 52 cells were used to assess pan-Rec8–GFP signals, 41 cells were used to assess MI focus and 43 cells were used to assess MII focus. For *quad*Δ 121 cells were used to assess pan-Rec8–GFP signals, 117 cells were used to assess MI focus and 117 cells were used to assess MII focus. **P*=2.95×10^{-9}, ***P*=7.91×10^{-17} (two-tailed *t*-test). (C) Representative western blot of Rec8–GFP and total protein determination of synchronous diploid meiosis using *pat1-114*/*mat2-102* for WT (6332×6336) and *quad*Δ (7402×7501). Each time point has between three and five biological replicates (see Materials and Methods; Table S3). The representative molecular mass markers (MW Standards) are shown for the first gel in the series of pictures. (D) Quantification of the ratio of Rec8–GFP phosphorylated form and total Rec8–GFP. Data are mean±s.e.m. **P*=0.0317 at time point −1 h (one-tailed Mann–Whitney test). (E) Quantification of Rec8–GFP protein levels by western blotting, calculated as the ratio of GFP signal to total protein. Data are mean±s.e.m. A one-tailed Wilcoxon test was used to determine significance from time points −4 h to −2 h (4 h to 2 h prior to MI completion): −4 h, *P*=0.0625; −3 h, *P*=0.125 and −2 h, *P*=0.0625. (F) ChIP of Rec8–GFP at *dh* or *act1*, from two biological replicates, for WT (6332×6336) and *quad*Δ (7402×7501). Data are mean±s.e.m. Strain numbers for parental strains in crosses are given in brackets, see Table S1 for details.

having reduced levels of Rec8–GFP at 4 h and 2 h prior to MI (Fig. 4E). Taken together, these data show that the *quad*Δ mutant has an observable change in Rec8–GFP dynamics in meiosis as well as a reduction in phosphorylation levels of Rec8.

One explanation for the reduced Rec8 protein levels in the live-cell imaging and reduced phosphorylation of Rec8 in the western blots is that Rec8 is not effectively deposited on the chromatin in the absence of the TLSPs. It is possible that Rec8 phosphorylation and

Journal of Cell Science (2020) 133, jcs238709. doi:10.1242/jcs.238709

subsequent cleavage requires that it is bound to the chromatin. In order to address the levels of Rec8–GFP bound to the chromatin we used chromatin immunoprecipitation (ChIP) to look at the centromere *dh* region and a distal euchromatic locus of *act1*. There was a significant reduction in Rec8–GFP at the pericentromeric region *dh* in the *quad*Δ compared to wild type (Fig. 4F). The effect is modest at early time points, but dramatic at later time points. Thus, the dynamics of Rec8–GFP at the centromere measured molecularly resemble the dynamics observed visually: premature removal of the Rec8–GFP cohesin from the centromere in the *quad*Δ mutant. There was no significant difference at the non-centromeric locus, *act1* (Fig. 4F). This does not resemble the dynamics observed visually. This may be due to the resolution of the time points taken. The delay in Rec8–GFP removal from the arms in the *quad*Δ mutant was ∼10 min, whereas the time points in the ChIP assay were every 2 h. It is important to note that we did not see the removal of Rec8–GFP at *act1* in the wild type. Additionally, MI and MII were seen to occur at 5 and 8 h, respectively, during *pat1-114*-driven meiosis (Fig. 2C). Taken together, these observations suggest that the time points used in the ChIP assay were not ideally suited to see Rec8–GFP removal from *act1* in wild type or to detect a delay in removal of Rec8–GFP. Interestingly, we did see a premature loss of Rec8–GFP at the centromere, indicating that in the *quad*Δ mutant Rec8 might be lost at the centromere prior to being lost at the arms.

In order to determine whether the disruption of meiotic cohesin in the *quad*Δ mutant is specific to meiotic-specific cohesins, we examined the dynamics of the mitotic cohesin Rad21 using a GFP-tagged version of the protein. In wild type, Rad21–GFP is visible in the 'horsetailing' phase of meiosis and disappears just before MI (Ding et al., 2006) (Fig. 5; Movie 5). The Rad21–GFP signal is localized to the leading edge of the horsetail nucleus in the rDNA region (Ding et al., 2006) (Fig. 5; Movie 5). There was no disruption in localization or timing detected in the *quad*Δ mutant compared to that in wild type (Fig. 5; Movies 5,6).

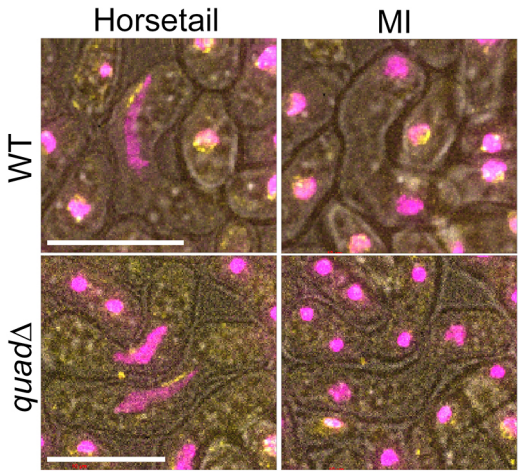

Fig. 5. Rad21–GFP in meiosis. Representative images of live-cell imaging of Rad21–GFP and H3–mRFP showing horsetailing and MI division for wild type (WT; 7644×7645) and *quad*Δ (7633×7634). Green shows Rad21–GFP and magenta shows H3–mRFP. Scale bars:10 µm. Images shown are representative of individual cells that were tracked independently on two separate days for *quad*Δ, and on a single day for WT.

DISCUSSION

We have shown that TLSPs contribute to chromosome segregation in meiosis, with an additive spore viability and inter-homolog recombination phenotype. In a *quad*Δ mutant lacking all four TLSPs in *S. pombe*, we observed defects in chromosome segregation in MI and MII leading to reduced spore viability. Spore viability of the *quad*Δ mutant was dramatically reduced compared to the single TLSP mutants (Fig. 1A), suggesting that there are overlapping functions of the TLSPs in meiosis. However, the same trend in spore viability was not observed for viability of mitotic cells (Fig. 1B).

These data do not support an essential role of TLSPs in meiotic recombination or DSB repair, at least in surviving cells. Normal levels of DSBs and their repair were observed and no changes in inter-homolog recombination rates were apparent in surviving cells (Fig. 2A,D). This does not discount the possibility that the TLSPs could be involved in a minor way that was undetectable by our methods, or that the inviable cells suffered irreversible damage due to failures in DSB repair. In budding yeast, TLSPs have been implicated in meiotic recombination and DSB repair by contributing to increased mutation rates around DSB sites (Arbel-Eden et al., 2013). Mutation rate at DSB sites were not tested in our study so the possibility that TLSPs are involved in this in *S. pombe* cannot be ruled out.

Defects in chromosome segregation during meiosis, as well as a disruption in the dynamics associated with the meiotic cohesin Rec8 were apparent in this study. Normally, Rec8 is removed from the chromosome arms but remains protected at the centromere in MI, finally being phosphorylated and cleaved to allow MII progression (Katis et al., 2010; Lee et al., 2005; Nasmyth and Haering, 2005; Watanabe, 2005; Watanabe and Kitajima, 2005). We observed a reduction of Rec8 meiosis-specific cohesin loading and/or maintenance at the pericentromeric region but no change at distal locations. Furthermore, the Rec8 that is loaded at the centromere appears unstable; there was no significant phosphorylation observed, yet it turned over more rapidly, especially following MI.

One possibility is that the TLSPs act as a recruitment or stabilization factor for Rec8. It has been shown that Rec8 is loaded to some extent prior to meiotic replication (Watanabe et al., 2001). Activation of cohesin occurs separately from loading and requires the acetyltransferase Eco1 (Kenna and Skibbens, 2003; Skibbens, 2005). Eco1 has been shown to interact directly with the replicative clamp (PCNA) and the clamp loader (RFC), implying a link between replication and cohesin activation (Kenna and Skibbens, 2003; Skibbens, 2005). Eco1 is required for the acetylation of the cohesin subunit Psm3, which localizes with Rec8 at the centromere in meiosis (Kagami et al., 2017). Without this acetylation, monopolar kinetochore attachment is inhibited (Kagami et al., 2017).

In *S. pombe*, *eso1* is a fusion of *polη* and the essential acetyltransferase homolog *eco1*, although the protein product may be split post-translationally (Chen et al., 2014). Still, at the transcriptional and translational levels these genes are co-regulated (Chen et al., 2014). This study did not robustly address the possibility that the deletion of the *polη* portion of *eso1* could have had a regulatory impact on Eco1 and thus could account for some of the meiotic defects observed. However, the fact that the spore viability of the *eso1*Δ*η* mutant was not greatly impacted, but in the *quad*Δ mutant there was a drastic reduction in spore viability, indicates that any misregulation of Eco1 due to the *polη* deletion does not account for the entirety of meiotic defects observed in the *quad*Δ mutant. In *Saccharomyces cerevisiae*, DNA Pol η is required for damage-induced genome-wide cohesion (Enervald et al., 2013). In that study there was no requirement for PCNA nor any of the other TLSPs in *S. cerevisiae* (Rev1 or Polζ) (Enervald et al., 2013). Additionally, *S. cerevisiae* DNA Pol κ is also linked to cohesion (Wang et al., 2000).

The premature loss of Rec8 in the TLSP quadruple mutant was accompanied by an increase in nondisjunction in MII. This is

Journal of Cell Science (2020) 133, jcs238709. doi:10.1242/jcs.238709

reminiscent of the phenotype observed for a non-cleavable form of Rec8, rather than that caused by loss of the protein (Kitajima et al., 2003). Thus, the presenting defect does not appear to be premature loss of centromere cohesion. An alternative interpretation of the MII nondisjunction could be that the lack of Rec8 at the centromere disrupts proper bipolar spindle attachment, as a residual amount of Rec8 at the centromere in MII is required for bipolar attachment of the kinetochore (Kitajima et al., 2004, 2006; Rabitsch et al., 2004; Riedel et al., 2006). If this is the explanation, then the apparent nondisjunction is due to an error in spindle attachment rather than an error in resolving cohesion. For example, destabilization of the centromere through deletion of *swi6* (a gene required for formation of pericentromeric heterochromatin) attenuates Rec8 loading, resulting in a mono-oriented kinetochore attachment in MII, leading to chromosome mis-segregation in MII (Kawashima et al., 2007; Kitajima et al., 2003; Yokobayashi et al., 2003). Interestingly, Swi6 is also required for the recruitment of Sgo1 and PP2A to the centromere through a direct interaction (Yamagishi et al., 2008). Thus, a disruption in centromeric structure could also cause the lack of Rec8 phosphorylation observed in this study.

The disruption observed in Rec8 meiosis-specific cohesin is not observed for Rad21. Rather, the Rad21 dynamics observed through live-cell imaging are normal. In *rec8*Δ there is an invasion of Rad21-GFP from the rDNA region into the chromosome arms (Ding et al., 2006). Even in the *rec8*Δ this effect is minor (Ding et al., 2006). It is then not surprising that there was not a detectible disruption of Rad21–GFP in the *quad*Δ, because Rec8 is largely retained in the *quad*Δ while its presence at the centromere is compromised.

A third possibility that remains is that the TLSPs may be required for efficient replication through the centromere and thus required for centromere stability in meiosis. In this case, a failure to segregate sister chromatids in MII could represent entanglements that link the chromosomes together due to unresolved replication intermediates or repair structures. There were no gross meiotic replication problems in the *quad*Δ mutant identified in this study; however, a more detailed analysis of replication at the centromere may be warranted.

MATERIALS AND METHODS

Cell growth and culture

General culture conditions and media are described in Sabatinos and Forsburg (2009) and Forsburg and Rhind (2006). Drug plates were incubated at 32°C for 2–4 days before being imaged using a flatbed scanner. For imaging, cells were concentrated in a fixed speed microfuge and spread on PMG agar on glass slides for imaging (Sabatinos et al., 2012). Heterothallic strains were grown independently for meiotic movies in PMG with appropriate supplements at 32°C until culture was in late log-phase (OD 595 nm ∼0.8). Cells were pelleted, washed in EMM medium minus the nitrogen source (EMM–N), and resuspended in ME and incubated 12-20 h in a 25°C shaking incubator. Cells were concentrated using a microfuge and spread on SPAS agar pads on glass slides. Imaging was performed at 25°C. Strains used are listed in Table S1. Sources of alleles for strains derived through crosses in this study are listed in Table S2.

Viability and recombination

Spore viability and recombination were performed by mating strains on SPAS agar for 2–3 days at which point the mating patch was scraped from a plate and diluted in 1 ml 0.5% glusulase (Perkin-Elmer, Catalog # NEE154001EA). This was digested for 16 h rotating at room temperature. Spores were plated on YES medium [as described in Forsburg and Rhind, (2006)] and grown at 32°C for 3–5 days before counting and replica plating colonies onto PMG media with appropriate supplements. Phloxin B (Sigma) was included to identify any diploids: no diploids or dyad asci were observed in TLSP mutants. His^+Lys^+ progeny were identified and genetic distance was calculated by (2(His^+Lys^+)/total colonies)×100. The experiment was repeated at least six times plating at least 1000 spores for each genotype each trial. Significance was calculated for genetic distances using a Student's two-tailed *t*-test. Mitotic viability was assayed via determining plating efficiency after cells were grown to an OD of ∼0.6 in YES medium at 32°C. The experiment was repeated at least six times for every genotype plating at least 1000 cells per trial.

Imaging

Images were acquired with a DeltaVision Core widefield deconvolution microscope (Applied Precision, Issaquah, WA) using an Olympus 60X/1.40, PlanApo, NA 1.40 objective lens and a 12-bit Photometrics CoolSnap HQII CCD, deep-cooled, Sony ICX-285 chip. The system *x*-*y* pixel size is 0.1092 µm. softWoRx v4.1 (Applied Precision, Issaquah, WA) software was used at acquisition electronic gain=1.0 and pixel binning 1×1. Excitation illumination was from a Solid-state illuminator (seven color version; Deltavision Core, Applied Precision Inc.), GFP was excited and detected with a (ex)475/28 nm, (em)525/50 nm filter set and a 0.2 s exposure; RFP was excited and detected with a (ex)575/25 nm, (em)632/60 nm filter set and a 0.2 s exposure. A suitable polychroic mirror (GFP/mRFP Chroma ET C125705) of roughly 520/50–630/80 nm was used. Thirteen *z* sections at 0.5 µm were acquired. 3D stacks were deconvolved with manufacturer provided OTFs using a constrained iterative algorithm and images were maximum intensity projected. Images were contrast adjusted using a histogram stretch with an equivalent scale and gamma for comparability. Brightfield images were acquired with DIC. Whole-cell SytoxGreen flow cytometry (FACS) was performed as described in Sabatinos and Forsburg (2009).

Western blotting

Cells were grown and synchronous meiosis was induced as in Catlett and Forsburg (2003). Cell cultures were stopped by adding 10× STOP buffer containing 2% sodium azide, 9% NaCl and 100 mM EDTA to harvested culture. The harvested culture was then incubated on ice for 10 min. Cells were washed in PBS buffer (137 mM NaCl, 2.7 mM KCl, 4.3 mM Na_2HPO_4 and 1.47 mM KH_2PO_4) and then Milli-Q water. Extracts were prepared using TCA (trichloroacetic acid; Foiani et al., 1994). Protein extracts were quantified using a Pierce BCA assay (Thermo Fisher Scientific). The linear range of detection was determined by loading different amounts of protein for the samples and blotting with the outline parameters. An amount of protein (50 µg) that was near the middle of the determined linear range was run on an 8% acrylamide with 1.25% crosslinker (Bio-Rad; 161-0140 and 161-0158) SDS–PAGE gel and transferred to a PVDF membrane. The membrane was probed with 5% BSA in Tris-buffered saline with 0.05% Tween 20 (TBST) containing a 1:2000 dilution of anti-GFP JL8 monoclonal antibodies (Clontech) overnight at 4°C, and washed three times for 5 min each in TBST. For the secondary antibody, blots were probed with TBST containing 5% milk and a 1:10,000 dilution of Alexa Flour 680-conjugated Goat anti-Mouse IgG (Fisher Scientific, A21057). Blots were visualized by scanning on the 700 nm channel using the LI-COR Odyssey Scanner. For measurements of total protein, 25 µg of the sample preparations were run on an 8% acrylamide gel with a 29:1 acrylamide to Bis ratio. The gels were stained using GelCode Blue stain reagent (Thermo Scientific, 24592). Gels were then scanned using the 700 nm channel with the LI-COR Odyssey Scanner. Blots and protein gels were quantified using Image Studio Light (LI-COR version 5.2.5). Rec8–GFP phosphorylation was measured as a ratio of the slower migrating species of Rec8–GFP to the total Rec8–GFP signal. Total protein was taken as the total signal in the lane. For all measurements, the background was subtracted using the auto background tool with settings that derived the background from the median of two pixels from the left and right of the box drawn. In order to determine synchrony and the timing of MI and MII in every experiment, ethanol-fixed cells were stained with DAPI and the nuclei were counted. Data is represented as MI being time zero because this is a defining feature to assess the progression of meiosis between experiments and strains. Between two and five biological replicates were used to determine Rec8–GFP phosphorylation levels and Rec8–GFP protein levels. For specific numbers of biological replicates used for each genotype in each experiment see Table S3.

Pulse-field gel electrophoresis

Synchronous diploid meiosis was achieved using the *mat2-102* and *pat1-114* alleles, as in Catlett and Forsburg (2003), to create stable diploids using *ade6-M210/M216* complementation. Pulse-field gel plugs were created by digesting the cell wall with 0.2 mg/ml 100T Zymolase (Seikagaku, Catalog # 120493-1) and 0.45 mg/ml Lysing Enzymes from *Aspergillus* sp. (Sigma, L3768) titrated to 50% and 25% of original strength for time points 1–2 and 3–6 respectively as in Cervantes et al. (2000). A pulse-field gel using a Biorad Chef II Pulse Field machine was run for 48 h using 2 V/cm, 1800 s switch time and a 106° angle. DNA was visualized via ethidium bromide staining.

ChIP

ChIP experiments followed a protocol modified from Le et al. (2013). Strains were harvested and cross-linked for 15 min with 1% formaldehyde at room temperature with rotating. Quenching was done with 0.25 mM glycine for 5 min at room temperature. Cells were harvested by centrifugation at 452.4 ***g*** for 3 min at 4°C and washed once with ice-cold Tris-buffered saline. Cells were resuspended in Tris-buffered saline and transferred to a screw-cap tube. After centrifugation, the supernatant was discarded, and the pellet was frozen and stored at – 80°C. Pellets were resuspended in 500 µl of lysis buffer [50 mm Hepes-KOH (pH 7.5), 150 mM NaCl, 1 mM EDTA, 1% Triton X-100, 0.1% sodium deoxycholate, 1× phosphatase inhibitor (Calbio) and 1× fungal protease inhibitor mixture (Sigma)], and cells were lysed by bead beating ten times for 1 min each with 5 min rests on ice. Tubes were punctured and spun into tubes for 1 min at 179.8 ***g***. The flow-through was transferred to a microcentrifuge tube and sonicated four times for 15 s each using a 12–15% amplitude duty cycle, resting on ice for 5 min in between sonications, to achieve shearing into fragments 500–750 bp in length. Samples were then spun at 20,000 ***g*** for 5 min at 4°C, the supernatant was transferred to a new tube and spun again for 10 min at 4°C. Supernatant was transferred to a new tube and quantified using Bradford reagent. A total of 1–2 mg crude lysate was diluted to 400 µl in ChIP lysis buffer and precleared using 30 µl Protein A beads (Invitrogen) rotating at 4°C for 2 h. A volume of 20 µl was set aside as the input control. A further 100 µl of the lysis buffer containing a 1:20 dilution of anti-GFP antibody (Abcam, ab290), or with no antibody (Mock), was added and rotated at 4°C overnight. Then, 15 µl of Protein A magnetic beads (NEB) were added to the lysate and rotated for 1 h at 4°C. Beads were washed twice for 5 min with lysis buffer, twice for 5 min each with high-salt lysis buffer (lysis buffer with 500 mM NaCl), once for 5 min with wash buffer [10 mM Tris-HCl (pH 8.0), 0.25 mM LiCl, 0.5% Nonidet P-40, 0.5% sodium deoxycholate and 1 mM EDTA] and once for 5 min with 10 mM Tris-HCl (pH 8.0) and 1 mM EDTA. Samples were eluted by addition of 100 µl of elution buffer [50 mM Tris-HCl (pH 8.0), 10 mM EDTA and 1% SDS] and incubated for 30 min at 65°C with agitation every 5 min. Sample crosslinking was reversed by incubation at 55°C overnight. Following this, 200 µg proteinase K was added and incubated at 37°C for 2 h. Samples were purified using a Qiagen PCR purification kit. DNA was quantified by end-point quantitative PCR with primers specific for the *dh* region and *act1*. Primer sequences used were as reported by Rougemaille et al. (2008). PCR products were separated using a 4% agarose gel and visualized via SYBR Green staining and scanning on biorad FX scanner. Quantification used GelEval Version 1.37 and calculated as (IP/Input) – (Mock/Input).

Acknowledgements

We thank members of the laboratory and Rachel Nieto for helpful comments.

Competing interests

The authors declare no competing or financial interests.

Author contributions

Conceptualization: T.L.M., S.L.F.; Methodology: T.L.M., S.L.F.; Validation: T.L.M., V.P.T.; Formal analysis: T.L.M.; Investigation: T.L.M., V.P.T.; Resources: S.L.F.; Writing - original draft: T.L.M.; Writing - review & editing: V.P.T., S.L.F.; Visualization: T.L.M.; Supervision: S.L.F.; Funding acquisition: S.L.F.

Funding

This work was supported by funding to S.L.F. from the National Institutes of Health (NIGMS R35 GM118109). Deposited in PMC for release after 12 months.

Supplementary information

Supplementary information available online at
http://jcs.biologists.org/lookup/doi/10.1242/jcs.238709.supplemental

Peer review history

The peer review history is available online at https://jcs.biologists.org/lookup/doi/10.1242/jcs.238709.reviewer-comments.pdf

References

Alexander, J. L. and Orr-Weaver, T. L. (2016). Replication fork instability and the consequences of fork collisions from rereplication. *Genes Dev.* **30**, 2241-2252. doi:10.1101/gad.288142.116

Arbel-Eden, A., Joseph-Strauss, D., Masika, H., Printzental, O., Rachi, E. and Simchen, G. (2013). Trans-lesion DNA polymerases may be involved in yeast meiosis. *G3 (Bethesda)* **3**, 633-644. doi:10.1534/g3.113.005603

Bähler, J., Schuchert, P., Grimm, C. and Kohli, J. (1991). Synchronized meiosis and recombination in fission yeast: observations with pat1-114 diploid cells. *Curr. Genet.* **19**, 445-451. doi:10.1007/BF00312735

Bavoux, C., Hoffmann, J. S. and Cazaux, C. (2005). Adaptation to DNA damage and stimulation of genetic instability: the double-edged sword mammalian DNA polymerase κ. *Biochimie* **87**, 637-646. doi:10.1016/j.biochi.2005.02.007

Bergoglio, V., Bavoux, C., Verbiest, V., Hoffmann, J.-S. and Cazaux, C. (2002). Localisation of human DNA polymerase kappa to replication foci. *J. Cell Sci.* **115**, 4413-4418. doi:10.1242/jcs.00162

Boddy, M. N., Gaillard, P.-H. L., McDonald, W. H., Shanahan, P., Yates, J. R. and Russell, P. (2001). Mus81-Eme1 are essential components of a Holliday junction resolvase. *Cell* **107**, 537-548. doi:10.1016/S0092-8674(01)00536-0

Brandão, L. N., Ferguson, R., Santoro, I., Jinks-Robertson, S. and Sclafani, R. A. (2014). The role of Dbf4-dependent protein kinase in DNA polymerase ζ-dependent mutagenesis in Saccharomyces cerevisiae. *Genetics* **197**, 1111-1122. doi:10.1534/genetics.114.165308

Callegari, A. J. and Kelly, T. J. (2016). Coordination of DNA damage tolerance mechanisms with cell cycle progression in fission yeast. *Cell Cycle* **15**, 261-273. doi:10.1080/15384101.2015.1121353

Callegari, A. J., Clark, E., Pneuman, A. and Kelly, T. J. (2010). Postreplication gaps at UV lesions are signals for checkpoint activation. *Proc. Natl. Acad. Sci. USA* **107**, 8219-8224. doi:10.1073/pnas.1003449107

Carvalho, C. M. B., Zhang, F. and Lupski, J. R. (2010). Evolution in health and medicine Sackler colloquium: genomic disorders: a window into human gene and genome evolution. *Proc. Natl. Acad. Sci. USA* **107**, 1765-1771. doi:10.1073/pnas.0906222107

Catlett, M. G. and Forsburg, S. L. (2003). Schizosaccharomyces pombe Rdh54 (TID1) acts with Rhp54 (RAD54) to repair meiotic double-strand breaks. *Mol. Biol. Cell* **14**, 4707-4720. doi:10.1091/mbc.e03-05-0288

Cervantes, M. D., Farah, J. A. and Smith, G. R. (2000). Meiotic DNA breaks associated with recombination in S. pombe. *Mol. Cell* **5**, 883-888. doi:10.1016/S1097-2765(00)80328-7

Chen, D., Toone, W. M., Mata, J., Lyne, R., Burns, G., Kivinen, K., Brazma, A., Jones, N. and Bähler, J. (2003). Global transcriptional responses of fission yeast to environmental stress. *Mol. Biol. Cell* **14**, 214-229. doi:10.1091/mbc.e02-08-0499

Chen, Z., Cao, H., Guo, W. and Lu, Y. (2014). Identification of two forms of the Eso1 protein in Schizosaccharomyces pombe. *Cell Biol. Int.* **38**, 682-688. doi:10.1002/cbin.10230

Coulon, S., Ramasubramanyan, S., Alies, C., Philippin, G., Lehmann, A. and Fuchs, R. P. (2010). Rad8Rad5/Mms2-Ubc13 ubiquitin ligase complex controls translesion synthesis in fission yeast. *EMBO J.* **29**, 2048-2058. doi:10.1038/emboj.2010.87

Cromie, G. A., Hyppa, R. W., Taylor, A. F., Zakharyevich, K., Hunter, N. and Smith, G. R. (2006). Single Holliday junctions are intermediates of meiotic recombination. *Cell* **127**, 1167-1178. doi:10.1016/j.cell.2006.09.050

Day, T. A., Palle, K., Barkley, L. R., Kakusho, N., Zou, Y., Tateishi, S., Verreault, A., Masai, H. and Vaziri, C. (2010). Phosphorylated Rad18 directs DNA polymerase η to sites of stalled replication. *J. Cell Biol.* **191**, 953-966. doi:10.1083/jcb.201006043

Deshpande, G. P., Hayles, J., Hoe, K.-L., Kim, D.-U., Park, H.-O. and Hartsuiker, E. (2009). Screening a genome-wide S. pombe deletion library identifies novel genes and pathways involved in genome stability maintenance. *DNA Repair* **8**, 672-679. doi:10.1016/j.dnarep.2009.01.016

Ding, D.-Q., Sakurai, N., Katou, Y., Itoh, T., Shirahige, K., Haraguchi, T. and Hiraoka, Y. (2006). Meiotic cohesins modulate chromosome compaction during meiotic prophase in fission yeast. *J. Cell Biol.* **174**, 499-508. doi:10.1083/jcb.200605074

Dolan, W. P., Le, A.-H., Schmidt, H., Yuan, J.-P., Green, M. and Forsburg, S. L. (2010). Fission yeast Hsk1 (Cdc7) kinase is required after replication initiation for induced mutagenesis and proper response to DNA alkylation damage. *Genetics* **185**, 39-53. doi:10.1534/genetics.109.112284

Enervald, E., Lindgren, E., Katou, Y., Shirahige, K. and Ström, L. (2013). Importance of Polη for damage-induced cohesion reveals differential regulation of

cohesion establishment at the break site and genome-wide. *PLoS Genet.* **9**, e1003158. doi:10.1371/journal.pgen.1003158
Escorcia, W. and Forsburg, S. L. (2017). Destabilization of the replication fork protection complex disrupts meiotic chromosome segregation. *Mol. Biol. Cell* **28**, 2978-2997. doi:10.1091/mbc.e17-02-0101
Foiani, M., Marini, F., Gamba, D., Lucchini, G. and Plevani, P. (1994). The B subunit of the DNA polymerase alpha-primase complex in Saccharomyces cerevisiae executes an essential function at the initial stage of DNA replication. *Mol. Cell. Biol.* **14**, 923-933. doi:10.1128/MCB.14.2.923
Forsburg, S. L. and Rhind, N. (2006). Basic methods for fission yeast. *Yeast* **23**, 173-183. doi:10.1002/yea.1347
Goodman, M. F. (2002). Error-prone repair DNA polymerases in prokaryotes and eukaryotes. *Annu. Rev. Biochem.* **71**, 17-50. doi:10.1146/annurev.biochem.71.083101.124707
Hastings, P. J., Ira, G. and Lupski, J. R. (2009). A microhomology-mediated break-induced replication model for the origin of human copy number variation. *PLoS Genet.* **5**, e1000327. doi:10.1371/journal.pgen.1000327
Heller, R. C. and Marians, K. J. (2006). Replication fork reactivation downstream of a blocked nascent leading strand. *Nature* **439**, 557-562. doi:10.1038/nature04329
Hochwagen, A. (2008). Meiosis. *Curr. Biol.* **18**, R641-R645. doi:10.1016/j.cub.2008.06.013
Ishiguro, T., Tanaka, K., Sakuno, T. and Watanabe, Y. (2010). Shugoshin-PP2A counteracts casein-kinase-1-dependent cleavage of Rec8 by separase. *Nat. Cell Biol.* **12**, 500-506. doi:10.1038/ncb2052
Kagami, A., Sakuno, T., Yamagishi, Y., Ishiguro, T., Tsukahara, T., Shirahige, K., Tanaka, K. and Watanabe, Y. (2017). Acetylation regulates monopolar attachment at multiple levels during meiosis I in fission yeast. *EMBO Rep.* **18**, 1263-1263. doi:10.15252/embr.201744401
Kai, M. and Wang, T. S.-F. (2003). Checkpoint activation regulates mutagenic translesion synthesis. *Genes Dev.* **17**, 64-76. doi:10.1101/gad.1043203
Katis, V. L., Lipp, J. J., Imre, R., Bogdanova, A., Okaz, E., Habermann, B., Mechtler, K., Nasmyth, K. and Zachariae, W. (2010). Rec8 phosphorylation by casein kinase 1 and Cdc7-Dbf4 kinase regulates cohesin cleavage by separase during meiosis. *Dev. Cell* **18**, 397-409. doi:10.1016/j.devcel.2010.01.014
Kawamoto, T., Araki, K., Sonoda, E., Yamashita, Y. M., Harada, K., Kikuchi, K., Masutani, C., Hanaoka, F., Nozaki, K., Hashimoto, N. et al. (2005). Dual roles for DNA polymerase η in homologous DNA recombination and translesion DNA synthesis. *Mol. Cell* **20**, 793-799. doi:10.1016/j.molcel.2005.10.016
Kawashima, S. A., Tsukahara, T., Langegger, M., Hauf, S., Kitajima, T. S. and Watanabe, Y. (2007). Shugoshin enables tension-generating attachment of kinetochores by loading Aurora to centromeres. *Genes Dev.* **21**, 420-435. doi:10.1101/gad.1497307
Kenna, M. A. and Skibbens, R. V. (2003). Mechanical link between cohesion establishment and DNA replication: Ctf7p/Eco1p, a cohesion establishment factor, associates with three different replication factor C complexes. *Mol. Cell. Biol.* **23**, 2999-3007. doi:10.1128/MCB.23.8.2999-3007.2003
Kim, S.-R., Maenhaut-Michel, G., Yamada, M., Yamamoto, Y., Matsui, K., Sofuni, T., Nohmi, T. and Ohmori, H. (1997). Multiple pathways for SOS-induced mutagenesis in Escherichia coli: an overexpression of dinB/dinP results in strongly enhancing mutagenesis in the absence of any exogenous treatment to damage DNA. *Proc. Natl. Acad. Sci. USA* **94**, 13792-13797. doi:10.1073/pnas.94.25.13792
Kitajima, T. S., Miyazaki, Y., Yamamoto, M. and Watanabe, Y. (2003). Rec8 cleavage by separase is required for meiotic nuclear divisions in fission yeast. *EMBO J.* **22**, 5643-5653. doi:10.1093/emboj/cdg527
Kitajima, T. S., Kawashima, S. A. and Watanabe, Y. (2004). The conserved kinetochore protein shugoshin protects centromeric cohesion during meiosis. *Nature* **427**, 510-517. doi:10.1038/nature02312
Kitajima, T. S., Sakuno, T., Ishiguro, K.-I., Iemura, S.-I., Natsume, T., Kawashima, S. A. and Watanabe, Y. (2006). Shugoshin collaborates with protein phosphatase 2A to protect cohesin. *Nature* **441**, 46-52. doi:10.1038/nature04663
Le, A.-H., Mastro, T. L. and Forsburg, S. L. (2013). The C-terminus of S. pombe DDK subunit Dfp1 is required for meiosis-specific transcription and cohesin cleavage. *Biol. Open* **2**, 728-738. doi:10.1242/bio.20135173
Lee, J. Y., Hayashi-Hagihara, A. and Orr-Weaver, T. L. (2005). Roles and regulation of the Drosophila centromere cohesion protein MEI-S332 family. *Philos. Trans. R Soc. Lond. B Biol. Sci.* **360**, 543-552. doi:10.1098/rstb.2005.1619
Li, X., Stith, C. M., Burgers, P. M. and Heyer, W.-D. (2009). PCNA is required for initiation of recombination-associated DNA synthesis by DNA polymerase delta. *Mol. Cell* **36**, 704-713. doi:10.1016/j.molcel.2009.09.036
Liu, P., Carvalho, C. M. B., Hastings, P. J. and Lupski, J. R. (2012). Mechanisms for recurrent and complex human genomic rearrangements. *Curr. Opin. Genet. Dev.* **22**, 211-220. doi:10.1016/j.gde.2012.02.012
Lorenz, A., Osman, F., Sun, W., Nandi, S., Steinacher, R. and Whitby, M. C. (2012). The fission yeast FANCM ortholog directs non-crossover recombination during meiosis. *Science* **336**, 1585-1588. doi:10.1126/science.1220111
Mastro, T. L. and Forsburg, S. L. (2014). Increased meiotic crossovers and reduced genome stability in absence of Schizosaccharomyces pombe Rad16 (XPF). *Genetics* **198**, 1457-1472. doi:10.1534/genetics.114.171355
Mata, J., Wilbrey, A. and Bähler, J. (2007). Transcriptional regulatory network for sexual differentiation in fission yeast. *Genome Biol.* **8**, R217. doi:10.1186/gb-2007-8-10-r217
McDonald, J. P., Rapić-Otrin, V., Epstein, J. A., Broughton, B. C., Wang, X., Lehmann, A. R., Wolgemuth, D. J. and Woodgate, R. (1999). Novel human and mouse homologs of Saccharomyces cerevisiae DNA polymerase eta. *Genomics* **60**, 20–30. doi:10.1006/geno.1999.5906
McIlwraith, M. J., McIlwraith, M. J., Vaisman, A., Liu, Y., Fanning, E., Woodgate, R. and West, S. C. (2005). Human DNA polymerase η promotes DNA synthesis from strand invasion intermediates of homologous recombination. *Mol. Cell* **20**, 783-792. doi:10.1016/j.molcel.2005.10.001
Nasmyth, K. and Haering, C. H. (2005). The structure and function of SMC and kleisin complexes. *Annu. Rev. Biochem.* **74**, 595-648. doi:10.1146/annurev.biochem.74.082803.133219
Ogi, T. and Lehmann, A. R. (2006). The Y-family DNA polymerase kappa (pol κ) functions in mammalian nucleotide-excision repair. *Nat. Cell Biol.* **8**, 640-642. doi:10.1038/ncb1417
Ohkura, H. (2015). Meiosis: an overview of key differences from mitosis. *Cold Spring Harbor Perspect. Biol.* **7**, a015859. doi:10.1101/cshperspect.a015859
Osman, F., Bjørås, M., Alseth, I., Morland, I., McCready, S., Seeberg, E. and Tsaneva, I. (2003). A new Schizosaccharomyces pombe base excision repair mutant, nth1, reveals overlapping pathways for repair of DNA base damage. *Mol. Microbiol.* **48**, 465-480. doi:10.1046/j.1365-2958.2003.03440.x
Ottaviani, D., LeCain, M. and Sheer, D. (2014). The role of microhomology in genomic structural variation. *Trends Genet.* **30**, 85-94. doi:10.1016/j.tig.2014.01.001
Pankratz, D. G. and Forsburg, S. L. (2005). Meiotic S-phase damage activates recombination without checkpoint arrest. *Mol. Biol. Cell* **16**, 1651-1660. doi:10.1091/mbc.e04-10-0934
Parisi, S., McKay, M. J., Molnar, M., Thompson, M. A., van der Spek, P. J., van Drunen-Schoenmaker, E., Kanaar, R., Lehmann, E., Hoeijmakers, J. H. and Kohli, J. (1999). Rec8p, a meiotic recombination and sister chromatid cohesion phosphoprotein of the Rad21p family conserved from fission yeast to humans. *Mol. Cell. Biol.* **19**, 3515-3528. doi:10.1128/MCB.19.5.3515
Prakash, S., Johnson, R. E. and Prakash, L. (2005). Eukaryotic translesion synthesis DNA polymerases: specificity of structure and function. *Annu. Rev. Biochem.* **74**, 317-353. doi:10.1146/annurev.biochem.74.082803.133250
Rabitsch, K. P., Gregan, J., Schleiffer, A., Javerzat, J.-P., Eisenhaber, F. and Nasmyth, K. (2004). Two fission yeast homologs of Drosophila Mei-S332 are required for chromosome segregation during meiosis I and II. *Curr. Biol.* **14**, 287-301. doi:10.1016/j.cub.2004.01.051
Rattray, A. J. and Strathern, J. N. (2005). Homologous recombination is promoted by translesion polymerase poleta. *Mol. Cell* **20**, 658-659. doi:10.1016/j.molcel.2005.11.018
Riedel, C. G., Katis, V. L., Katou, Y., Mori, S., Itoh, T., Helmhart, W., Gálová, M., Petronczki, M., Gregan, J., Cetin, B. et al. (2006). Protein phosphatase 2A protects centromeric sister chromatid cohesion during meiosis I. *Nature* **441**, 53-61. doi:10.1038/nature04664
Rougemaille, M., Shankar, S., Braun, S., Rowley, M. and Madhani, H. D. (2008). Ers1, a rapidly diverging protein essential for RNA interference-dependent heterochromatic silencing in Schizosaccharomyces pombe. *J. Biol. Chem.* **283**, 25770-25773. doi:10.1074/jbc.C800140200
Rumpf, C., Cipak, L., Dudas, A., Benko, Z., Pozgajova, M., Riedel, C. G., Ammerer, G., Mechtler, K. and Gregan, J. (2010). Casein kinase 1 is required for efficient removal of Rec8 during meiosis I. *Cell Cycle* **9**, 2657-2662. doi:10.4161/cc.9.13.12146
Ryan, A. J., Squires, S., Strutt, H. L., Evans, A. and Johnson, R. T. (1994). Different fates of camptothecin-induced replication fork-associated double-strand DNA breaks in mammalian cells. *Carcinogenesis* **15**, 823-828. doi:10.1093/carcin/15.5.823
Sabatinos, S. A. and Forsburg, S. L. (2009). Measuring DNA content by flow cytometry in fission yeast. *Methods Mol. Biol.* **521**, 449-461. doi:10.1007/978-1-60327-815-7_25
Sabatinos, S. A., Green, M. D. and Forsburg, S. L. (2012). Continued DNA synthesis in replication checkpoint mutants leads to fork collapse. *Mol. Cell. Biol.* **32**, 4986-4997. doi:10.1128/MCB.01060-12
Sakofsky, C. J., Ayyar, S., Deem, A. K., Chung, W.-H., Ira, G. and Malkova, A. (2015). Translesion polymerases drive microhomology-mediated break-induced replication leading to complex chromosomal rearrangements. *Mol. Cell* **60**, 860-872. doi:10.1016/j.molcel.2015.10.041
Sharif, W. D., Glick, G. G., Davidson, M. K. and Wahls, W. P. (2002). Distinct functions of S. pombe Rec12 (Spo11) protein and Rec12-dependent crossover recombination (chiasmata) in meiosis I; and a requirement for Rec12 in meiosis II. *Cell Chromosome* **1**, 1.
Skibbens, R. V. (2005). Unzipped and loaded: the role of DNA helicases and RFC clamp-loading complexes in sister chromatid cohesion. *J. Cell Biol.* **169**, 841-846. doi:10.1083/jcb.200503129
Tanaka, K., Yonekawa, T., Kawasaki, Y., Kai, M., Furuya, K., Iwasaki, M., Murakami, H., Yanagida, M. and Okayama, H. (2000). Fission yeast Eso1p is

required for establishing sister chromatid cohesion during S phase. *Mol. Cell. Biol.* **20**, 3459-3469. doi:10.1128/MCB.20.10.3459-3469.2000

Tomita, K. and Cooper, J. P. (2007). The telomere bouquet controls the meiotic spindle. *Cell* **130**, 113-126. doi:10.1016/j.cell.2007.05.024

Wang, Z., Castaño, I. B., Las Peñas, A., Adams, C. and Christman, M. F. (2000). Pol kappa: a DNA polymerase required for sister chromatid cohesion. *Science* **289**, 774-779. doi:10.1126/science.289.5480.774

Watanabe, Y. (2005). Shugoshin: guardian spirit at the centromere. *Curr. Opin. Cell Biol.* **17**, 590-595. doi:10.1016/j.ceb.2005.10.003

Watanabe, Y. and Kitajima, T. S. (2005). Shugoshin protects cohesin complexes at centromeres. *Philos. Trans. R. Soc. Lond. B Biol. Sci.* **360**, 515-521. doi:10.1098/rstb.2004.1607

Watanabe, Y. and Nurse, P. (1999). Cohesin Rec8 is required for reductional chromosome segregation at meiosis. *Nature* **400**, 461-464. doi:10.1038/22774

Watanabe, Y., Yokobayashi, S., Yamamoto, M. and Nurse, P. (2001). Pre-meiotic S phase is linked to reductional chromosome segregation and recombination. *Nature* **409**, 359-363. doi:10.1038/35053103

Waters, L. S., Minesinger, B. K., Wiltrout, M. E., D'Souza, S., Woodruff, R. V. and Walker, G. C. (2009). Eukaryotic translesion polymerases and their roles and regulation in DNA damage tolerance. *Microbiol. Mol. Biol. Rev.* **73**, 134-154. doi:10.1128/MMBR.00034-08

Yamagishi, Y., Sakuno, T., Shimura, M. and Watanabe, Y. (2008). Heterochromatin links to centromeric protection by recruiting shugoshin. *Nature* **455**, 251-255. doi:10.1038/nature07217

Yokobayashi, S., Yamamoto, M. and Watanabe, Y. (2003). Cohesins determine the attachment manner of kinetochores to spindle microtubules at meiosis I in fission yeast. *Mol. Cell. Biol.* **23**, 3965-3973. doi:10.1128/MCB.23.11.3965-3973.2003

Zeman, M. K. and Cimprich, K. A. (2014). Causes and consequences of replication stress. *Nat. Cell Biol.* **16**, 2-9. doi:10.1038/ncb2897

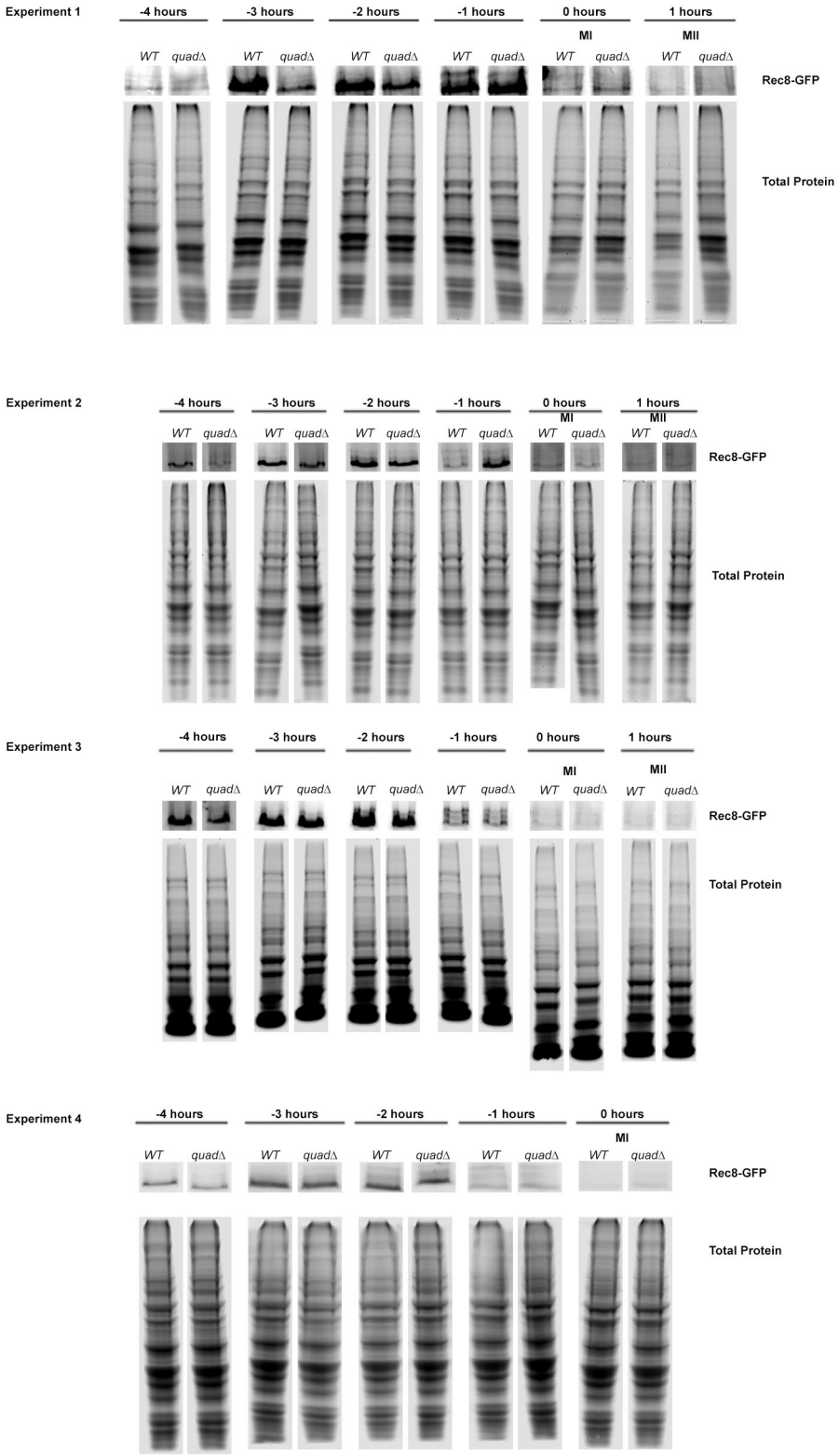

Figure S1: Western Blots of Rec8-GFP. This figure is related to Figure 4. Blots and total protein gels used in determining Rec8-GFP phosphorylation and abundances. Only one gel technical replicate for Experiment 1 is pictured although two technical replicates were completed and averaged. Experiment 5 is not pictured as there was only data for WT time points from -2, -1, and 0 available for analysis.

Movie 1: Live cell imaging of WT chromosome segregation. Representative live cell imaging of WT (5608x5787) heterozygote LacI-GFP and *lacO* at centromere I with H3-mRFP in meiosis. Yellow is LacI-GFP and magenta is H3-mRFP.

Movie 2: Live cell imaging of *quad*Δ chromosome segregation. Representative live cell imaging of *quad*Δ (6671x7117) heterozygote LacI-GFP and *lacO* at centromere I with H3-mRFP in meiosis. Yellow is LacI-GFP and magenta is H3-mRFP.

Movie 3: Live cell imaging of WT Rec8 cohesin. Representative live cell imaging of WT (6137x6138) with Rec8-GFP in meiosis. Green is Rec8-GFP.

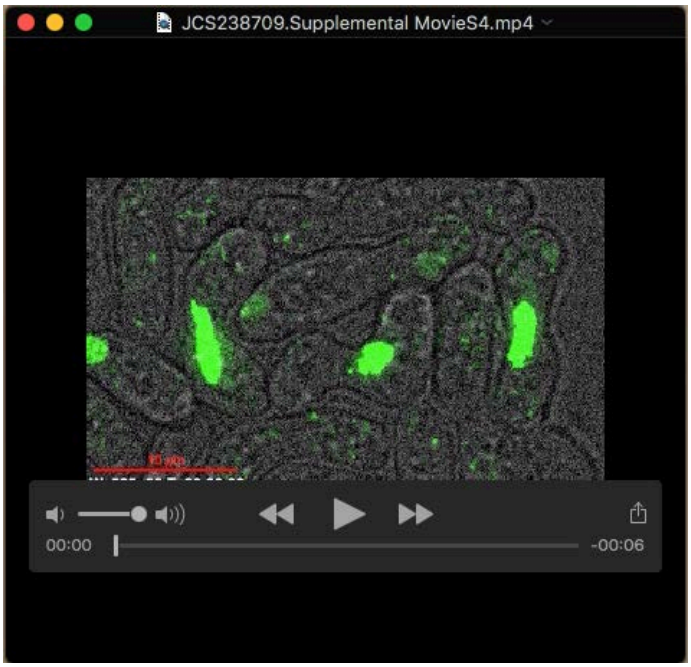

Movie 4: Live cell imaging of *quad*Δ Rec8 cohesin. Representative live cell imaging of *quad*Δ (7428x7402) with Rec8-GFP in meiosis. Green is Rec8-GFP.

Movie 5: Live cell imaging of WT Rad21 cohesin. Representative live cell imaging of WT (7644x7645) with Rad21-GFP and H3-mRPF in meiosis. Yellow is Rad21-GFP and magenta is H3-mRFP

Movie 6: Live cell imaging of *quad*Δ Rad21 cohesin. Representative live cell imaging of *quad*Δ (7633x7634) with Rad21-GFP and H3-mRPF in meiosis. Yellow is Rad21-GFP and magenta is H3-mRFP

Table S1: Strains used in this study.

Strain	Genotype	Source
1251	*h+ ade6-M26 his4-239*	Gerry Smith
2057	*h- pat1-114 ade6-M216 can1-1*	Mastro 2014
3070	*h- Δrad3::ura4+ ura4-D18*	Lab Stock
3500	*h90 mat2-102 pat1-114 ade6-M210*	Mastro 2014
4561	*h+ Δrec12::ura4+ ura4-D18 his4-239 ade6-M26*	This Study
5207	*h- lys4-95 ade6-52*	Mastro 2014
5258	*h- Δkpa1::bleMX6 lys4-95 ade6-52*	This Study
5259	*h- Δrev3::hphMX6 lys4-95 ade6-52*	This Study
5262	*h- eso1Δη ::kanMX6 lys4-95 ade6-52*	This Study
5263	*h+ Δrev3::hghMX6 his4-239 ade6-M26*	This Study
5268	*h- Δrec12::ura4+ ura4-D18 ade6-52 lys4-95*	This Study
5269	*h+ eso1Δη::kanMX6 his4-239 ade6-M26*	This Study
5401	*h+ Δrev1::ura4+ ura4-D18 his4-239 ade6-M26*	This Study
5466	*h- Δrev1::ura4+ ura4-D18 lys4-95 ade6-52*	This Study
5608	*h- hht1-mRFP:KanMX6 leu1-32 ura4-D18*	Mastro 2014
5787	*h+ hht1-mRFP:kanMX his7+::lacI-GFP lys1+::lacO leu1-32 ura4-D18*	Mastro 2014
6173	*h+ rec8-GFP-kan(YW) leu1-32 ade6-M210*	This Study
6174	*h- rec8-GFP-kan(YW) leu1-32 ade6-M210*	This Study
6332	*h90 mat2-102 pat1-114 rec8-GFP-kan(YW) ade6-M210*	Mastro 2014
6336	*h- pat1-114 rec8-GFP-kan(YW) ade6-M216*	Mastro 2014
6664	*h- his4-239 eso1Δη::kanMX6 Δkpa1::bleMX6 Δrev3::hphMX6 Δrev1::ura4+ ura-D18 ade6-*	This Study
6671	*h90 mat2-101 pat1-114 eso1η::kanMX6 Δkpa1::bleMX6 Δrev3::hphMX6 Δrev1::ura4+ ura-D18 leu1-32 ade6-M210*	This Study
6703	*h+ eso1Δη::kanMX6 Δkpa1:bleMX6 Δrev3::hphMX6 Δrev1::ura4+ ura-D18 his4-239 ade6-m26?*	This Study
6716	*h+ eso1Δη::kanMX6 Δkpa1:bleMX6 Δrev3::hphMX6 Δrev1::ura4+ ura-D18 lys4-95 ade6-52*	This Study
6717	*h- eso1Δη::kanMX6 Δkpa1:bleMX6 Δrev3::hphMX6 Δrev1::ura4+ ura-D18 lys4-95 ade6-52*	This Study
7117	*h- eso1Δη::kanMX6 Δkpa1::bleMX6 Δrev3::hphMX6 Δrev1::ura4+ his7+::lacI-GFP lys1+::lacO hht1-mRFP:natMX6 ura4-D18 leu1-32 ade6-*	This Study
7167	*h- pat1-114 eso1Δη::kanMX6 Δkpa1::bleMX6 Δrev3::hphMX6 Δrev1::ura4+ ura-D18 leu1-32 ade6-M216*	This Study
7168	*h+ eso1Δη::kanMX6 Δkpa1::bleMX6 Δrev3::hphMX6 Δrev1::ura4+ hht1-mRFP:natMX6 ura4-D18 leu1-32 ade6-*	This Study
7402	*h- pat1-114 rec8-GFP::kanMX6 eso1Δη::kanMX6 Δkpa1::bleMX6 Δrev3::hphMX6 Δrev1::ura4+ ura-D18 ade6-M216*	This Study
7501	*h90 mat2-102 pat1-114 eso1Δη::kanMX6 kpa1Δ::bleMX6 rec8-gfp:kanMX rev3::hphMX6 Δrev1::ura4+ ura-D18 ade6-M210*	This Study
7616	*h+ Δkpa1:bleMX6 his4-239 ade6-*	This Study

7633	*h- leu1 rad21-GFP[leu2] eso1Δη::kanMX6 Δkpa1::bleMX6 Δrev3::hphMX6 Δrev1::ura4+ hht1-mRFP:natMX6 ura4-D18 leu1-32 ade6(-)?*	This Study
7634	*h+ leu1 rad21-GFP[leu2] eso1Δη::kanMX6 Δkpa1::bleMX6 Δrev3::hphMX6 Δrev1::ura4+ hht1-mRFP:natMX6 ura4-D18 leu1-32 ade6(-)?*	This Study
7644	*h- leu1 rad21-GFP[leu2] hht1-mRFP:kanMX*	This Study
7645	*h+ leu1 rad21-GFP[leu2] hht1-mRFP:kanMX*	This Study
7685	*h- Δkpa1:bleMX6 lys4-95 ade6-*	This Study
7691	*h- eso1Δη::kanMX6 Δkpa1::bleMX6 Δrev3::hphMX6 Δrev1::ura4+ taz1-GFP::kanMX6 hht1-mRFP:KanMX6 ura4-D18 leu1-32 ade6(-)?*	This Study
7692	*h+ eso1Δη::kanMX6 Δkpa1::bleMX6 Δrev3::hphMX6 Δrev1::ura4+ taz1-GFP::kanMX6 hht1-mRFP:KanMX6 ura4-D18 leu1-32 ade6(-)?*	This Study

Table S2: Allele Sources for strains derived through crosses in this study.

Allele	**Source**
Δ*rev3*::hphMX6	Derived from Matthew O'Connell's #2753
eso1Δη ::kanMX6	Matthew O'Connell's #2751
Δ*rev1*::ura4+	Derived from Thomas Kelly's AJC-F53
Δ*kpa1*:bleMX6	Matthew O'Connell's #2752
hht1-mRFP:KanMX6	Derived from Julie Cooper's JCF5474
his7+::lacI-GFP lys1+::lacO	Derived from strain from M. Yanagida. Described in (Nabeshima et al., 1998)
rec8-GFP-kan	Derived from Y. Watanabe (PY204)
Rad21-GFP[leu2]	Derived from yeast genetic resource center japan FY10969
Taz1-GFP::kanMX6	Derived from Yasushi Hiraoka. Described in (Chikashige and Hiraoka, 2001)

Table S3: Biological replicate numbers used in western blotting.

	Rec8-GFP Phosphorylation		**Rec8-GFP / Total Protein**	
Time Point	**WT**	**quadΔ**	**WT**	**quadΔ**
-6	n/a	n/a	4	3
-5	n/a	n/a	4	4
-4	4	4	4	4
-3	4	4	4	4
-2	5	4	4	4
-1	5	4	4	4
0	5	4	4	4
1	3	3	3	3
2	n/a	n/a	2	2